



43 [13] found that the NIR reflectance band is less sensitive for determining vegetation cover (or  
44 vegetation fraction – VF), for VF >60%, and showed that a VI using the green-red-blue wavelengths  
45 have a linear relationship to VF, with an accuracy level of up to 90%. They showed that in Wheat,  
46 when VF is between 50-100%, the green wavelength is most sensitive to changes in vegetation cover  
47 (while the blue, red and NIR wavelengths were insensitive to changes in vegetation cover).

48 [14] found that the green to red (G/R) spectral wavelengths ratio index is sensitive to the  
49 amount of greenness of the plant: it is less than 1 in the beginning and at the end of the growing  
50 season, and above 1 at midseason [14,15]. [15] concluded that the G/R ratio may serve as a  
51 benchmark for crop growth, phenological stages and for indicating VF.

52 Another VI that is based on the G/R ratio is the Green-Red Vegetation Index (GRVI) that is  
53 defined according to Eq. 1:

$$54 \quad \text{GRVI} = (\rho_{\text{green}} - \rho_{\text{red}}) / (\rho_{\text{green}} + \rho_{\text{red}}) \quad (1)$$

55 [16] evaluated the use of GRVI as a phenological indicator. They concluded that the GRVI index can  
56 differentiate between green vegetation (index above 0), water and snow (index around 0) and soils  
57 (index below 0). Furthermore they demonstrated that GRVI (unlike NDVI) is sensitive to leaf color  
58 change (leaf green-up and autumn coloring). They suggested using the threshold of GRVI=0 as a site  
59 specific threshold for monitoring phenological changes, and the GRVI index as an indicator for plant  
60 disturbances and comparing between different ecosystem types [16].

61 Current satellite-based remotely sensed products can cover large areas, but is limited both by its  
62 temporal (revisit time) and spatial (pixel size) resolutions, when compared to unmanned aerial  
63 vehicle (UAV). One of satellite imaging's challenges is dealing with pixels that have multiple objects  
64 with different spectral signatures (e.g. plants and soil). Such pixels are called mixed-pixels. UAV  
65 imaging high spatial resolution, produces mixed-free pixels, therefore making vegetation detection  
66 and differentiation an easier task. Similarly, high spatial resolution allows for precise estimation of  
67 vegetation cover fraction.

68 A basic method for irrigation scheduling is factoring the potential evapo-transpiration (PET),  
69 computed from measured radiation, wind speed, air temperature and relative humidity, with a  
70 crop specific coefficient (Kc), [17]. Crop coefficients are provided by diverse methods, such as  
71 empirical conclusions from field experiments, degree days based seasonal functions, experts'  
72 recommendations, and the FAO #56 publication Kc library; or by field specific measurements. Since  
73 the evapotranspiration (ET) driving energy received by the crop canopy is directly proportional to  
74 the light interception (LI) [18,19], and LI is directly proportional to crop cover, Kc can be fitted to  
75 field and plot specific dimension by measuring crop cover. Aerial surveys derived VF is directly  
76 proportional to cover, [20] thus aerial photography provides efficient method to Kc determination.

77 The main objective of this study was to test the ability of an inexpensive RGB camera mounted  
78 on an inexpensive unmanned aerial vehicle (UAV) to determine vegetation cover and vigor at the  
79 canopy scale in a large scale whole field resolution, and to investigate whether vegetation cover and  
80 vigor patterns can be utilized as indicators to irrigation water application uniformity. Another  
81 objective of this study was to compare the efficiency of an RGB based VI, with the well-known  
82 NDVI, both in UAV based high spatial resolution cameras and also via satellite imaging.

## 83 2. Materials and Methods

### 84 2.1 UAV imaging system

85 DJI Phantom 4 quadcopter UAV was used as the flying platform. The UAV is equipped with a  
86 built-in RGB camera with 4000x3000 pixel 4K resolution CMOS sensor, 20mm (35 mm eq.) lens with  
87 FOV of 94°, in a 3-axis stabilized gimbal. The UAV was flown using Pix4D Capture pre-programmed  
88 flightpath control. The Parrot Sequoia multispectral sensor was used in order to compare NDVI with  
89 GRVI. The Parrot Sequoia sensor consist of five downward looking image sensors: Visible 16 MPixel  
90 (RGB) with a definition of 4608x3456 pixels, and four 1.2 MPixel: Green (550 nm), Red (660 nm), Red

91 Edge (735 nm), and Near infrared (790 nm) bands, 1280x960 pixels. The sensor was mounted on a DJI  
92 Mavic-Pro small size foldable rotors quadcopter UAV.

## 93 2.2 Flight campaigns

94 Flight campaigns were conducted in two test sites: at the Gadot center pivot test site (33°  
95 2'22.91"N , 35°38'0.43"E), and at the Havat Gadash field crops experimental farm (33°10'56.24"N ,  
96 35°35'5.78"E), both located in the Upper Galilee region in within the northern part of Israel. The area  
97 has a Mediterranean climate, characterized by wet, mild winters, and hot, dry summers. Annual  
98 winter rainfall in the range of 400-600 mm, while summer crops utilize 80-120 mm of winter soil  
99 water storage for initial growth periods. The field at the Gadot center pivot test site was cultivated  
100 with cotton crop, sown on April 4, 2017. The field was irrigated at 8 days intervals beginning from  
101 June 3. Two flight campaigns were conducted on July 5, and August 24, when the crop has already  
102 reached full cover. The flights were conducted at mid-day, at 50m altitude, and pixel spatial  
103 resolution of 0.02m. At the Havat Gadash Peanuts cv *Hanoach* were sown on May 1, 2017 and  
104 irrigated uniformly by an experimental lateral move, starting at May 8 (**Table 1**). PET was calculated  
105 according to the Penman-Montieth formula. Four differential irrigation treatments: 120%, 100%, 85%  
106 and 70% replacement of PET, starting on July 19. Prior to this date, uniform irrigation was applied to  
107 all treatments (**Table 1**). The Kc (70%) treatment yielded the highest, and was selected for ground  
108 truth validation. Experimental plots were 12x25m four plots side by side in 4 replicates. Seven flight  
109 campaigns were conducted at mid-day, at 10-50m altitude, and pixel spatial resolution of  
110 0.006-0.02m. Crop cover didn't reach full cover during the first two campaigns (June 25, July 17).

111 Table 1: Cumulative ET, irrigation water applied, and Kc in the peanut irrigation experiment, Havat  
112 Gadash 2017.

	Date	Cumulative ET (mm) *	Irrigation (mm)	Cumulative irrigation (mm) *	Kc **
Uniform irrigation	04/06/2017	170	40	40	0.23
	13/06/2017	230	40	80	0.35
	29/06/2017	342	45	125	0.37
	06/07/2017	389	45	170	0.44
	12/07/2017	432	45	215	0.50
0.7 Kc Irrigation	19/07/2017	43	37	37	0.86
	27/07/2017	96	37	74	0.77
	03/08/2017	143	37	111	0.78
	10/08/2017	186	37	148	0.80
	19/08/2017	240	37	185	0.77
	30/08/2017	308	37	222	0.72
	10/09/2017	369	37	259	0.70
	24/09/2017	434	40	299	0.69

\* Cumulative amounts recalculated for the two experimental stages  
\*\* Kc calculated as cumulative irrigation divided by cumulative ET

113 Flight courses were created with the Pix4Dcapture software, which was also used to  
114 automatically pilot the DJI Phantom 4 UAV according to the flight path. Overlap percentage of 60%  
115 was chosen in order to ease the task of mosaicking.

116 In order to compare between NDVI and GRVI, a flight campaign using the DJI Mavic-Pro UAV  
117 was conducted in the peanut field at the Havat Gadash experimental farm, on October 10, twelve  
118 days before the end of the growing season. The Parrot Sequoia multispectral sensor was used to  
119 create the NDVI, while the RGB camera was used to create the GRVI.

## 120 2.3 Data processing

121 The images collected in each flight campaign were mosaicked and georeferenced using the  
122 Pix4Dmapper software. ArcGIS 10.5 geo-referencing tools were used for fine adjustments.

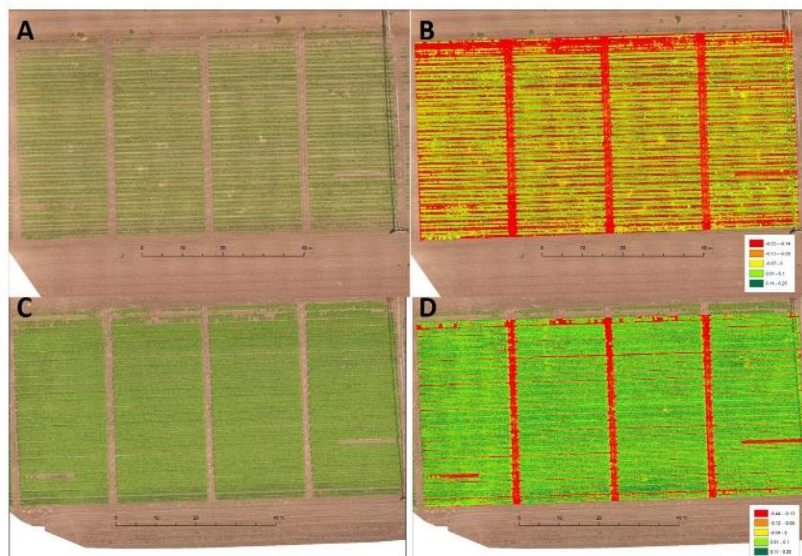
123 VF was calculated using ArcGIS 10.5, calculating the histogram of the GRVI products. Pixels  
124 with GRVI values greater than 0 were classified as vegetation. At the beginning of the growing  
125 season, negative values that were close to 0 were also classified as vegetation.

126 Sentinel-2 Level-2A atmospherically corrected images of the Gadot test site from August 29,  
127 2017 were acquired courtesy of the Copernicus Open Access Hub. Several VI were created and  
128 compared to the UAV image from August 24, in order to check whether it is possible to use  
129 Sentinel-2 satellite imaging (with spatial resolution of 10m) to determine irrigation uniformity  
130 issues. The VI that were checked are: NDVI [5], GNDVI [9] and GRVI [5,16].

### 131 3. Results and discussion

#### 132 3.1 Havat Gadash experimental farm campaign

133 The RGB images (**Fig. 1A,C**) have high spatial resolution from which crop can be differentiated  
134 from soil. The GRVI images reveal crop phenological stages: most of the vegetation pixels' GRVI  
135 values in the image taken 55 days from sowing are around zero, and even slightly below zero (**Fig.**  
136 **1B**), G/R ratio is close to one and even less than 1 – indicative to the beginning of the growing season.  
137 On the other hand, most of the vegetation pixels' GRVI values in the later image from 77 days from  
138 sowing (**Fig. 1D**) are above zero, indicative to healthy and vital vegetation suitable to midseason  
139 phenological stage. Therefore, GRVI is also helpful in determining phenological stages. The VF  
140 determined according to the GRVI images histograms was 40% and 80% (**Fig. 1B,D** respectively).  
141 The calculated  $K_c$  for the campaign dates (**Table 1**) are in-par with the calculated VF, validating the  
142 VF calculations.



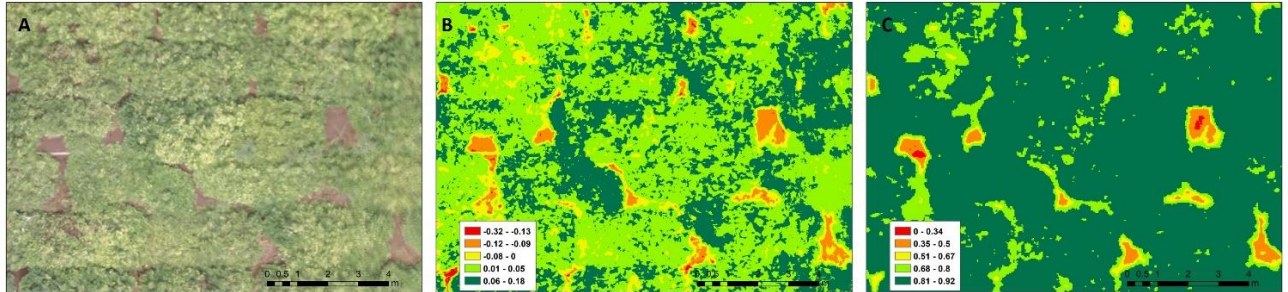
143  
144 Figure 1: RGB (A+C) and GRVI (B+D) images of the peanut field in Havat Gadash experimental farm  
145 on 25/6 (A+B, 55 days from sowing), and on 17/7 (C+D, 77 days from sowing).

#### 146 3.2 Comparison between NDVI and GRVI

147 Since there are 2 different sensors measuring the NDVI and the GRVI (**section 2.3**), the spatial  
148 resolution of the NDVI is lower (pixel size of 0.0373m) than that of the GRVI (0.0095m). thus  
149 enabling sharper GRVI imagery. The image was taken toward the end of the season, depicting plants  
150 in different stages of senescence. As can be seen in **Fig. 2**, GRVI captures plant senescence better than  
151 the NDVI: changes in plant color from green to yellow is depicted more accurately in the GRVI  
152 image, when compared to the NDVI image. Greener vegetation (depicted in the RGB image **Fig. 2A**)  
153 has higher GRVI values (**Fig. 2B**). On the other hand, the NDVI image (**Fig. 2C**) doesn't capture the



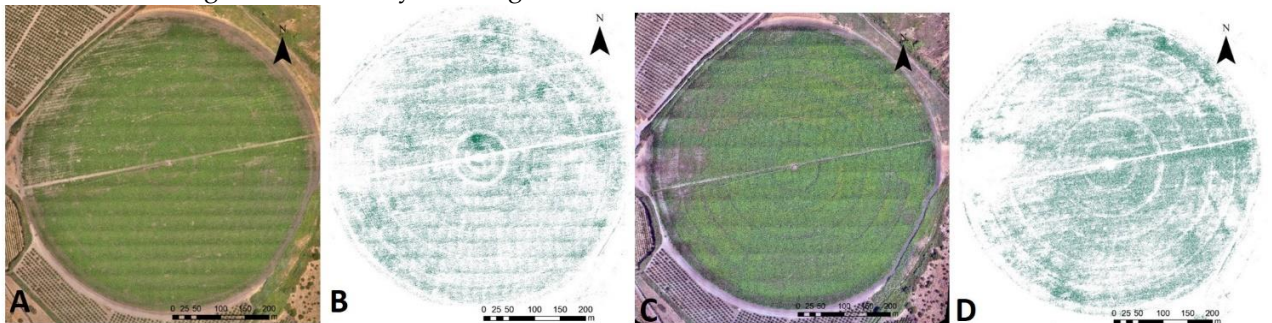
154 differences between plants that are visible in the RGB image (**Fig. 2A**). NDVI values are very high for  
155 most pixels, indicating saturation of NDVI values, probably due to high LAI values [7,11,12]. It is  
156 probable that differences in pixel resolution are also responsible for the accuracy differences.  
157 Regardless, for the purpose of vegetation classification and vigor analysis, the use of RGB VI is better  
158 than the NDVI, thus making the Parrot-Sequoia NIR sensor superfluous.



159  
160 Figure 2: RGB (A), GRVI (B) and NDVI (C) zoom-in images of the peanut field at Havat Gadash  
161 experimental farm.

### 162 3.3 Gadot test site campaign

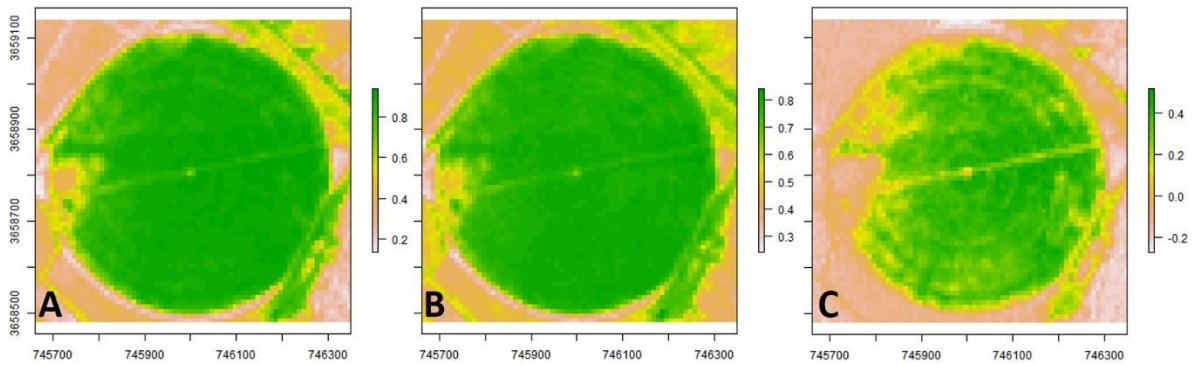
163 The images of the Gadot pivot irrigated cotton crop were taken after the crop has reached full  
164 canopy cover (**Fig. 3A,C**). A closer look at the GRVI images can reveal “sector” lines, indicating  
165 differences in plant vigor (**Fig. 3B,D**). The “sector” patterns are an indicative of ununiformed  
166 irrigation, due to intermittent pivot movement: the “greener” areas probably received more  
167 irrigation, due to lower pivot speed. This could be resulted from physical obstacles, uneven ground,  
168 malfunctioning pivot control, etc. Whereas these “sectors” are noticeably visible by the GRVI image,  
169 it’s impossible to notice them from the RGB image. Therefore using the GRVI in this case is crucial in  
170 order to detect irrigation uniformity and irrigation malfunctions and other subtle disturbances.



171  
172 Figure 3: RGB (A+C) and GRVI (B+D) images of the cotton field in Gadot test site on 05/07 (A+B), and  
173 on 24/08 (C+D).

### 174 3.4 Sentinel-2 satellite VI of Gadot test site

175 The NDVI and GNDVI images are pretty similar, showing high values homogenously  
176 throughout the whole field, except the middle left corner (**Fig. 4A,B**). The GRVI image is more  
177 heterogeneous, showing patches of low values, that are correlated to the UAV high resolution GRVI  
178 image’s patches (**Fig. 4C, Fig. 3D**), indicative of the field’s heterogeneity of plant vigor and  
179 ununiformed irrigation. The GRVI is therefore better at presenting the real crop vigor situation.  
180 Whereas Saturation of red reflectance at intermediate to high Chlorophyll values is well known  
181 [10,15] and is indicative to NDVI, it is surprising to see that the GNDVI is also saturated and  
182 doesn’t show the field’s heterogeneity.



183

184

185

Figure 4: NDVI (A), GNDVI (B), and GRVI (C) vegetation indexes based on a Sentinel-2 imagery of the cotton field in Gadot test site from 29/08/2017

186

#### 4. Conclusions

187

188

189

190

191

192

193

194

195

196

197

198

199

200

201

In this study the ability of a high resolution RGB imaging to determine vegetation cover and vigor at the canopy scale in a large scale whole field resolution was evaluated, using an RGB VI, the GRVI. It was concluded that the GRVI is suitable for determining vegetation cover, distinguishing between vegetation and other land covers (such as soil and dead vegetation, **Fig. 1**). VF can be accurately measured and be used by the farmer “on the spot” in order to directly define Kc. It was also shown that the GRVI can be used to distinguish plant’s phenological stages: detecting early season and senescence is easy with GRVI: when GRVI is lower than 0, that’s a sign for low plant’s vigor; when GRVI is greater than zero, this indicated strong plant vigor and is indicative to mid-season plant phenological stage (**Fig. 1-2**). It was also concluded that GRVI is better than NDVI and GNDVI in detecting subtle disturbances in mid-season period (**Fig. 4**). High resolution RGB imaging can be utilized to monitor irrigation water application uniformity, and to detect heterogeneity in field irrigation (**Fig. 3**). Since both the camera and the UAV used in this research are inexpensive and available, and with current auto-pilot UAV existing technologies easing the use of UAVs, the presented tools should be available for “on the spot” farming decision making processes involving precision irrigation and irrigation management.

202

#### References

203

204

205

206

207

208

209

210

211

212

213

214

215

216

217

218

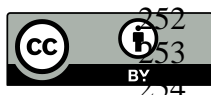
219

220

221

1. Hatfield, J. L.; Gitelson, A. A.; Schepers, J. S.; Walthall, C. L. Application of spectral remote sensing for agronomic decisions. *Agronomy Journal* **2008**, *100*, doi:10.2134/agronj2006.0370c.
2. Hunt, E. R.; Doraiswamy, P. C.; McMurtrey, J. E.; Daughtry, C. S. T.; Perry, E. M.; Akhmedov, B. A visible band index for remote sensing leaf chlorophyll content at the Canopy scale. *International Journal of Applied Earth Observation and Geoinformation* **2012**, *21*, 103–112, doi:10.1016/j.jag.2012.07.020.
3. Jordan, C. F. Derivation of Leaf-Area Index from Quality of Light on the Forest Floor. *Ecology* **1969**, *50*, 663–666, doi:10.2307/1936256.
4. Rouse, J. W.; Hass, R. H.; Schell, J. A.; Deering, D. W. Monitoring vegetation systems in the great plains with ERTS. *Third Earth Resources Technology Satellite (ERTS) symposium* **1973**, *1*, 309–317, doi:citeulike-article-id:12009708.
5. Tucker, C. J. Red and photographic infrared linear combinations for monitoring vegetation. *Remote Sensing of Environment* **1979**, *8*, 127–150, doi:10.1016/0034-4257(79)90013-0.
6. Huete, A. R. A soil-adjusted vegetation index (SAVI). *Remote Sensing of Environment* **1988**, *25*, 295–309, doi:10.1016/0034-4257(88)90106-X.
7. Hunt, E. R.; Daughtry, C. S. T.; Eitel, J. U. H.; Long, D. S. Remote sensing leaf chlorophyll content using a visible band index. *Agronomy Journal* **2011**, *103*, 1090–1099, doi:10.2134/agronj2010.0395.
8. Yoder, B. J.; Waring, R. H. The normalized difference vegetation index of small Douglas-fir canopies with varying chlorophyll concentrations. *Remote Sensing of Environment* **1994**, *49*, 81–91, doi:10.1016/0034-4257(94)90061-2.

- 222 9. Gitelson, A. A., Kaufman, Y. J., & Merzlyak, M. N. Use of a green channel in remote sensing of global  
223 vegetation from EOS-MODIS. *Remote Sensing of Environment* **1996**, *58*, 289–298,  
224 doi:10.1016/S0034-4257(96)00072-7.
- 225 10. Gitelson, A. A.; Viña, A.; Ciganda, V.; Rundquist, D. C.; Arkebauer, T. J. Remote estimation of canopy  
226 chlorophyll content in crops. *Geophysical Research Letters* **2005**, *32*, 1–4, doi:10.1029/2005GL022688.
- 227 11. Daughtry, C. S. T.; Walthall, C. L.; Kim, M. S.; De Colstoun, E. B.; McMurtrey Iii, J. E. Estimating Corn Leaf  
228 Chlorophyll Concentration from Leaf and Canopy Reflectance. *Remote Sensing of Environment* **2000**, *74*,  
229 229–239, doi:10.1016/S0034-4257(00)00113-9.
- 230 12. Eitel, J. U. H.; Long, D. S.; Gessler, P. E.; Hunt, E. R.; Brown, D. J. Sensitivity of Ground-Based Remote  
231 Sensing Estimates of Wheat Chlorophyll Content to Variation in Soil Reflectance. *Soil Science Society of*  
232 *America Journal* **2009**, *73*, 1715, doi:10.2136/sssaj2008.0288.
- 233 13. Gitelson, A. A.; Kaufman, Y. J.; Stark, R.; Rundquist, D. Novel algorithms for remote estimation of  
234 vegetation fraction. *Remote Sensing of Environment* **2002**, *80*, 76–87, doi:10.1016/S0034-4257(01)00289-9.
- 235 14. Adamsen, F. J.; Pinter, P. J.; Barnes, E. M.; LaMorte, R. L.; Wall, G. W.; Leavitt, S. W.; Kimball, B. A.  
236 Measuring wheat senescence with a digital camera. *Crop Science* 1999, *39*, 719–724.
- 237 15. Kanemasu, E. T. Seasonal canopy reflectance patterns of wheat, sorghum, and soybean. *Remote Sensing of*  
238 *Environment* **1974**, *3*, 43–47, doi:10.1016/0034-4257(74)90037-6.
- 239 16. Motohka, T.; Nasahara, K. N.; Oguma, H.; Tsuchida, S. Applicability of Green-Red Vegetation Index for  
240 remote sensing of vegetation phenology. *Remote Sensing* **2010**, *2*, 2369–2387, doi:10.3390/rs2102369.
- 241 17. Allen, R. G.; Pereira, L. S.; Raes, D.; Smith, M.; Ab, W. Crop evapotranspiration (guidelines for computing  
242 crop water requirements), FAO Irrigation and Drainage Paper No. 56. *FAO, Rome*. **1998**, 290,  
243 doi:10.1016/j.eja.2010.12.001.
- 244 18. Johnson, R. S.; Ayars, J.; Trout, T.; Mead, R.; Phene, C. Crop coefficients for mature peach trees are well  
245 correlated with midday canopy light interception. *Acta Horticulturae* 2000, *537*, 455–460.
- 246 19. Green, S.; McNaughton, K.; Wünsche, J. N.; Clothier, B. Modeling Light Interception and Transpiration of  
247 Apple Tree Canopies. *Agronomy Journal* **2003**, *95*, 1380, doi:10.2134/agronj2003.1380.
- 248 20. Meron M., Tsipris J., Hetsroni A., C. S. Aerial photography and ground based equipment to evaluate crop  
249 cover for tree specific irrigation scheduling. in: *D. Mulla (Ed.), 8th International Conference on Precision*  
250 *Agriculture Minneapolis MN USA. pp. CD 2006*.
- 251



© 2018 by the authors; licensee MDPI, Basel, Switzerland. This article is an open access article distributed under the terms and conditions of the Creative Commons Attribution (CC-BY) license (<http://creativecommons.org/licenses/by/4.0/>).